12
Applications

Figures

12.2 Measuring the optical constants of metals

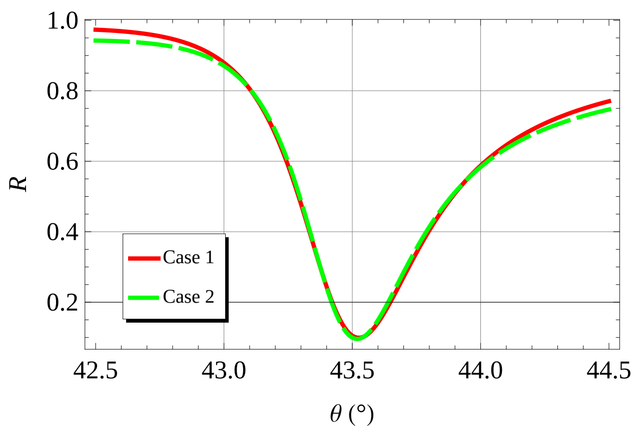

Fig. 12.1. Theoretical reflectivity as a function of angle of incidence, θ, for two films with different refractive indices and thicknesses measured in the Kretschmann configuration at a fixed wavelength of 632.8 nm. Case 1 corresponds to a film of thickness 38.7 nm and dielectric constant -17.45 + i 0.92. Case 2 corrseponds to a film of thickness 48.3 nm and dielectric constant -16.72 + i 1.66. (*Mathematica* simulation.)

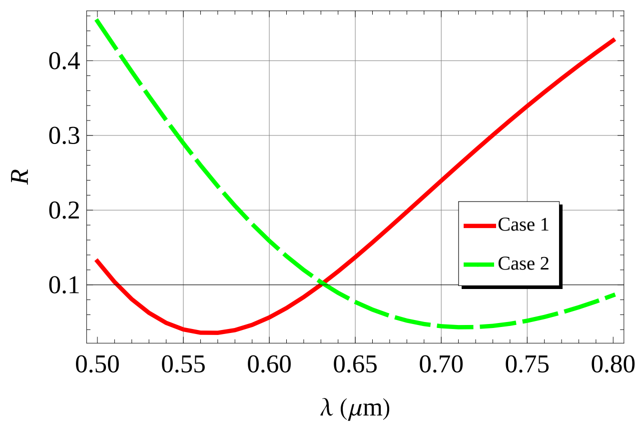

Fig. 12.2. Theoretical reflectivity as a function of wavelength, λ, for the same two films of Fig. 12.1 measured in the Kretschmann configuration at a fixed angle of 43.5°. (*Mathematica* simulation.)

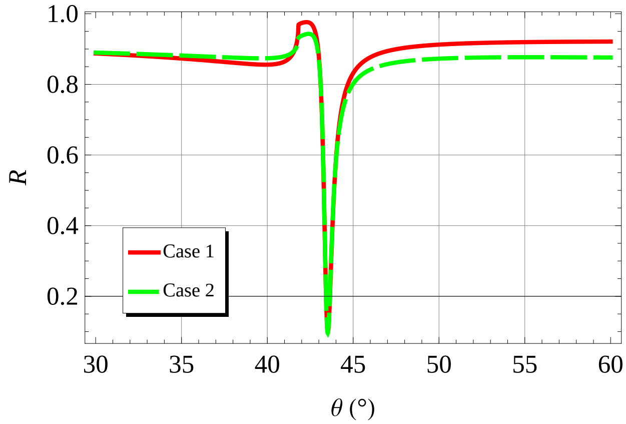

Fig. 12.3. Theoretical reflectivity as a function of angle of incidence, θ, for the same two films in Fig. 12.1 measured in the Kretschmann configuration at a fixed wavelength of 632.8 nm. (*Mathematica* simulation).

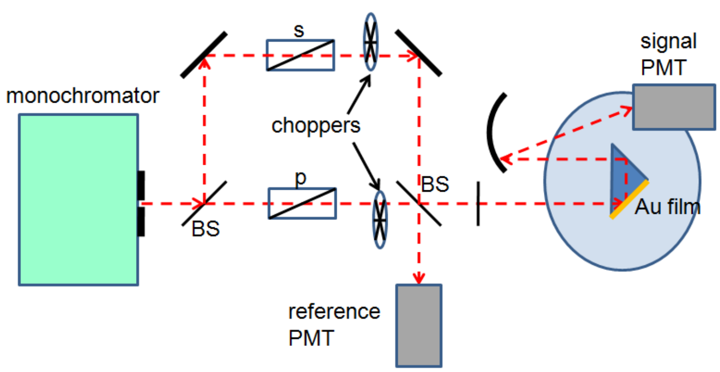

Fig. 12.4. Apparatus for measuring the optical constants of metallic films using the Kretschmann configuration. Light from the monochromator is divided into two beams which are polarized in orthogonal directions and modulated by choppers at different frequencies. A second beamsplitter sends some of the recombined beam to the sample, which is a gold film on a prism mounted on a rotation stage, and then on to a detector. The other half of the beam goes directly to a second detector. The two signals are demodulated by lock-in amplifiers. Adapted from [3].

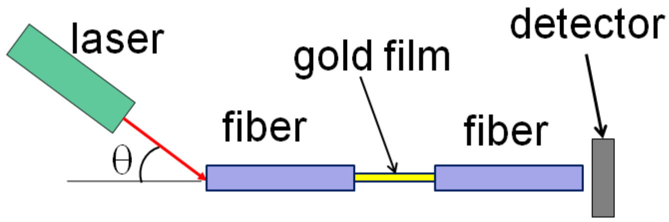

Fig. 12.5. Fiber optic technique for measuring the optical constants of metallic films. The cladding is removed over a distance of 15 mm along the fiber and the core is coated with the metal film.

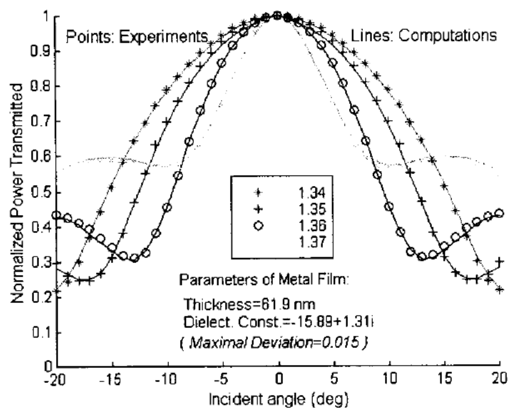

Fig. 12.6. Transmitted power as a function of angle of incidence for a gold film deposited onto the core of a fiber. The fiber is immersed in solutions with refractive indices of 1.34, 1.35, 1.36 and 1.37. Used by permission. [4]

12.3 Chemical and biological sensors

12.3.2 Kretschmann sensors

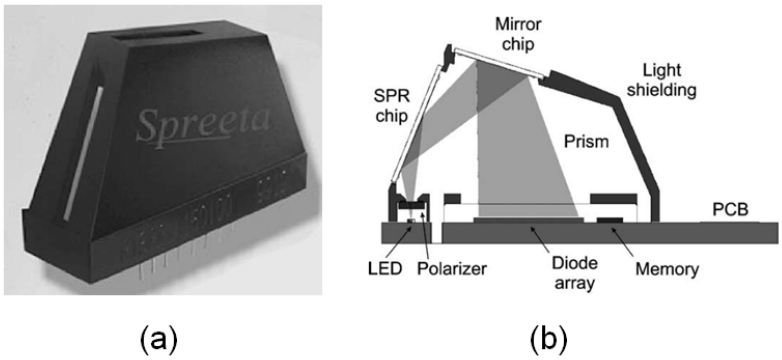

Fig. 12.7. (a) Spreeta SPR sensor developed by Texas Instruments, and (b) cut-away view of the internal design. Reprinted from *Sensors and Actuators B*, **91**, T.M. Chinowsky, J.G. Quinn, D.U. Bartholomew, R. Kaiser, and J.L. Elkind, "Performance of the Spreeta 2000 integrated surface plasmon resonance affinity sensor," 266-274, © 2003, with permission from Elsevier. [6]

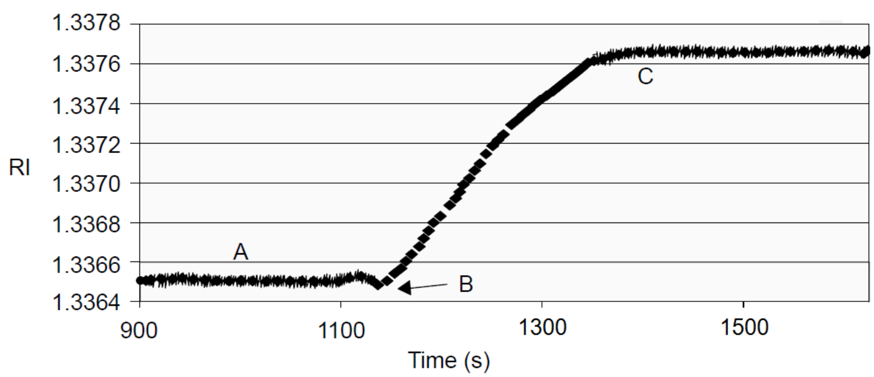

Fig. 12.8. Effective change in refractive index due to the binding interaction of biotinylated anti-DNP antibodies in phosphate-buffered saline solution to a gold surface prepared with neutravidin as a function of time. The vertical scale is in units of refractive index, RI. Courtesy Texas Instruments. [8]

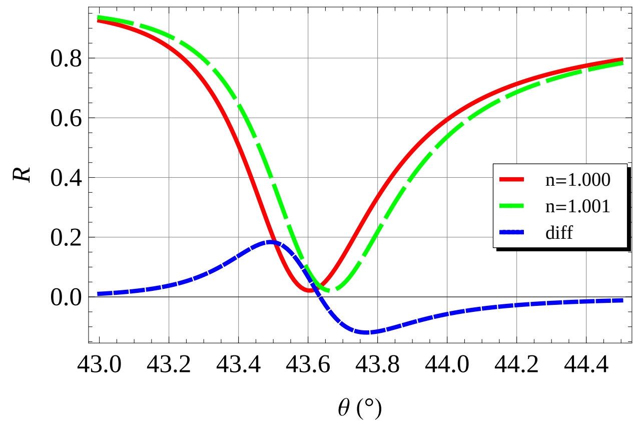

Fig. 12.9. Reflectivity of a silver surface as a function of angle of incidence, θ, in the Kretschmann configuration for vacuum (n = 1.0, solid line) and a gas with a refractive index of 1.001 (long dashes). The shift in the resonant angle is clearly visible. At the angle of incidence of 43.5°, the change in the reflectivity (short dashes) is nearly 20%. (*Mathematica* simulation.)

12.3.3 Nanoparticle sensors

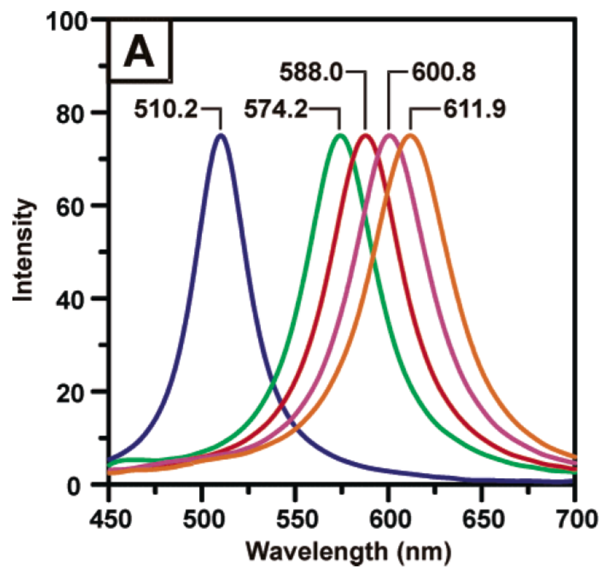

Fig. 12.10. Scattering spectra for Ag nanoparticles when immersed in gases/liquids of various refractive indices. From left to right these are nitrogen, methanol, 1-propanol, chloroform and benzene. Reprinted with permission from [9]. © 2003 American Chemical Society.

12.3.4 Optical fiber sensors

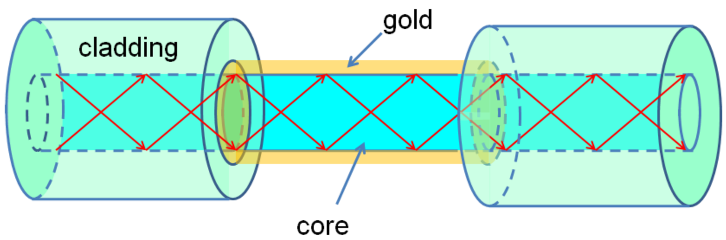

Fig. 12.11. SP resonance sensor made from an optical fiber. A thin gold film is deposited on a bare segment of the fiber core. A broad spectrum of light is transmitted through the fiber and generates a SP on the outer surface of the gold film at the correct wavelength.

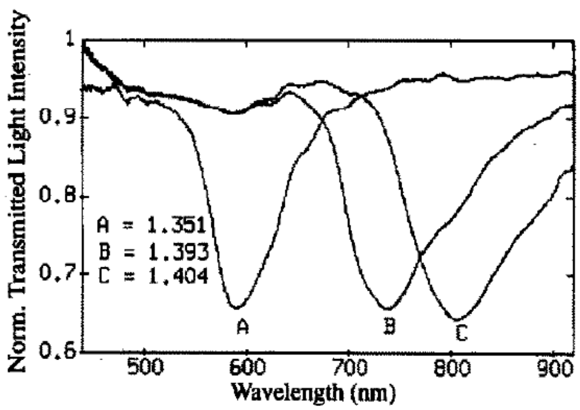

Fig. 12.12. Spectrum of transmitted light for an optical fiber SPR sensor as the refractive index of the liquid surrounding the silver film is varied. Reprinted from *Sensors and Actuators B*, **12**, R. C. Jorgenson and S. S. Yee, "A fiber-optic chemical sensor based on surface-plasmon resonance," (1993) 213. © 1993, with permission from Elsevier. [13]

12.4 Near field microscopy

12.4.1 Scanning plasmon near field microscopy

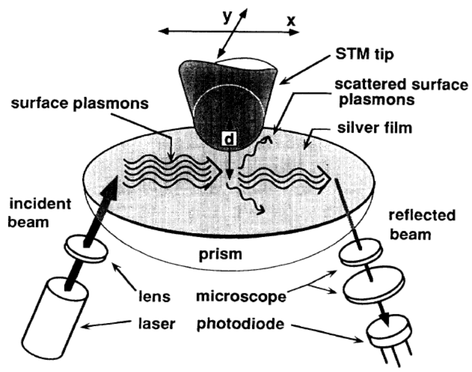

Fig. 12.13. Apparatus for scanning plasmon near field microscopy. Reprinted with permission from M.Specht, J. D. Pedarnig, W. M. Heckl and T. W. Hänsch, *Phys. Rev. Lett.* **68** 476 (1992). © 1992 by the American Physical Society. [15]

12.4.2 Photon scanning tunneling microscopy

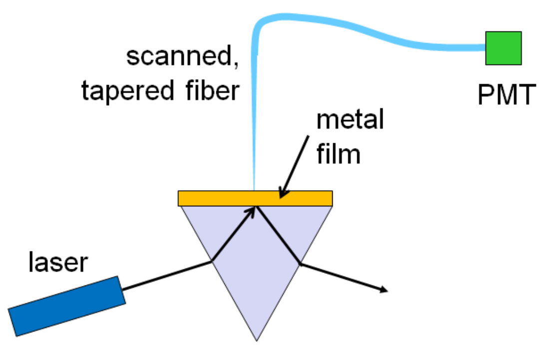

Fig. 12.14. Apparatus for photon scanning tunneling microscopy. After *Opt. Commun.* **117** , S. I. Bozhevolnyi, B. Vohnsen, I. I. Smolyaninov, A. V. Zayats, "Direct observation of surface polariton localization caused by surface roughness," (1995) 417. © 1995, with permission from Elsevier.

12.4.3 Fiber-based scanning near field microscopy with a nanoparticle

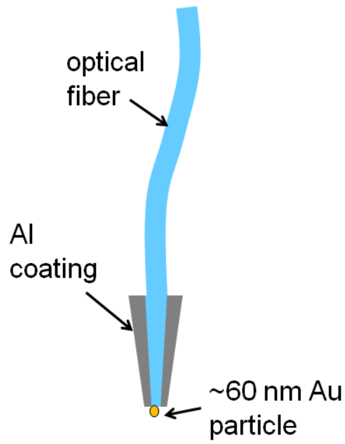

Fig. 12.15. Probe for optical fiber-based scanning near field optical microscopy.

12.4.4 Fiber-based scanning near field microscopy with an aperture

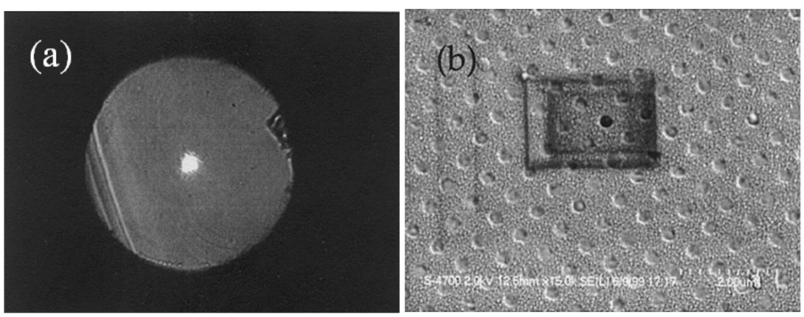

Fig. 12.16. (Left) End of fiber probe for optical fiber-based scanning near field optical microscopy. (Right) Magnified view of silver film on end of fiber showing dimple array with center hole. Reprinted from *Physica B* **279**, T. Thio, H.J. Lezec and T. W. Ebbesen, "Strongly enhanced optical transmission through subwavelength holes in metal films" 90. © 2000, with permission from Elsevier. [18]

12.4.5 The superlens

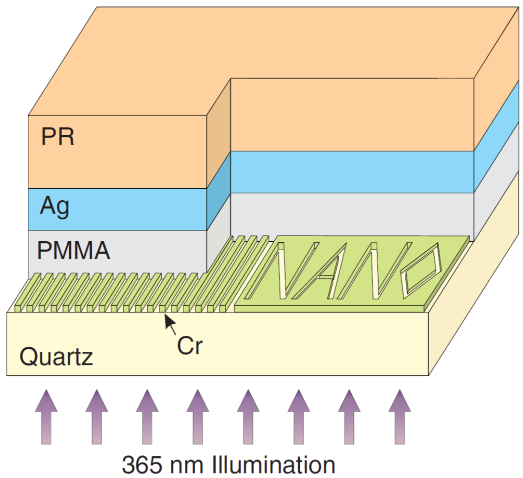

Fig. 12.17. Structure used to demonstrate a superlens. A Cr film deposited onto a quartz substrate was patterned with a grating and the letters "NANO." It was overcoated with a PMMA spacer, a 35 nm silver film, and photoresist. 365 nm radiation from a mercury lamp was used to expose the photoresist through the substrate. From N. Fang, H. Lee, C. Sun and X. Zhang, *Science* **308** (2005) 534. Reprinted with permission from AAAS. [21]

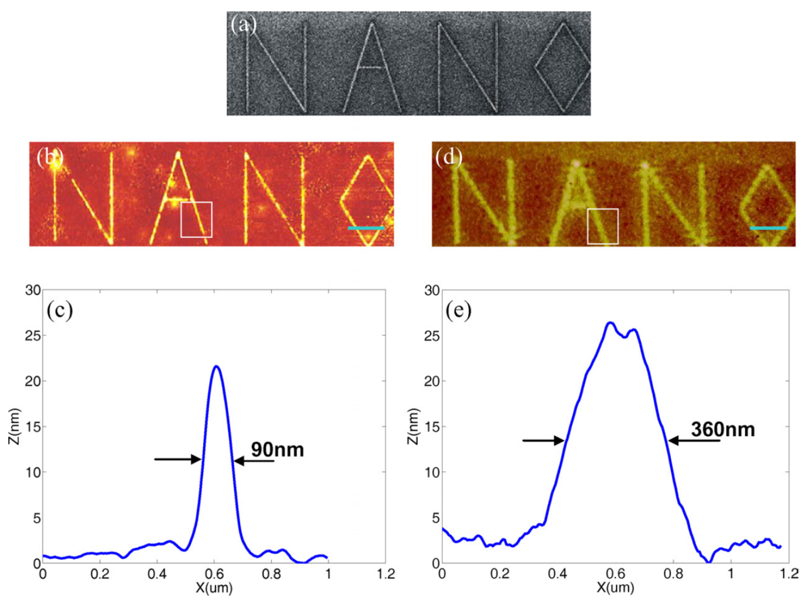

Fig. 12.18. (a) FIB image of the pattern in the Cr layer. (b) Exposed pattern in the photoresist above the superlens silver layer and (c) averaged AFM line scan of the leg of the letter "A" with a FWHM width of 90 nm. (d) Control experiment in which the silver was replaced by PMMA and (e) averaged AFM line scan of the leg of the letter "A" with a width of 360 nm. The scale bar in (a), (b), and (d) is 100 nm. Used by permission of IOP Publishing Ltd. [22]

12.5 Surface enhanced Raman spectroscopy

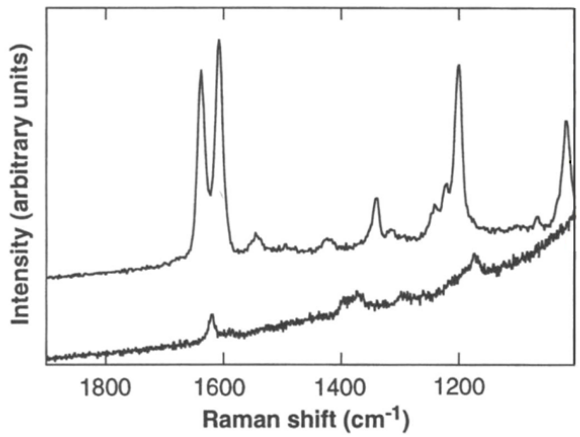

Fig. 12.19. Comparison of SERS spectrum of *trans*-1,2-bis(4-pyridyl)ethylene on a colloidal gold substrate (top) to the Raman spectrum the same solution on a bare SiO_x TEM grid (bottom). From R. G. Freeman *et al.*, *Science* **267** (1995) 1629. Reprinted with permission from AAAS. [38]

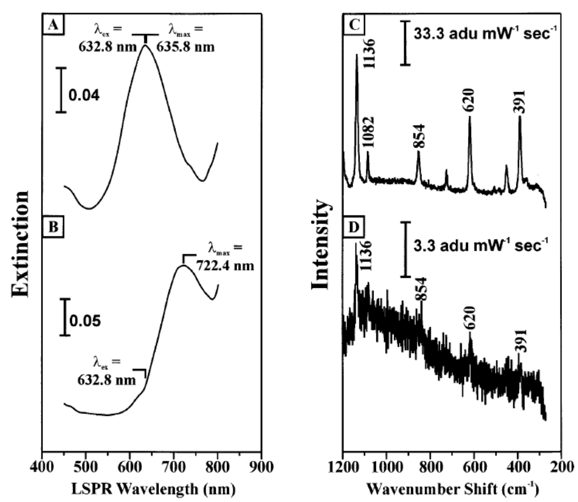

Fig. 12.20. (Left) Measured extinction coefficient of the silver nanoparticles. The top plot is for 56 nm particles and the bottom plot is for 20 nm nanoparticles. (Right) Measured SERS spectra for the same silver nanoparticles. A strong spectrum is observed when the incident laser wavelength at 632.8 nm lies at the SP resonance, while a very weak spectrum is observed when the incident laser wavelength is not resonant. Reprinted with permission from [41], © 2003 American Chemical Society.

12.6 Nonlinear optics

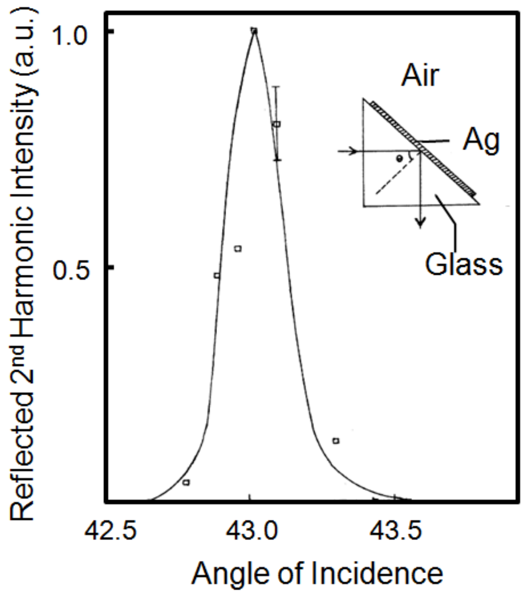

Fig. 12.21. Intensity of second harmonic light generated at a silver surface in the Kretschmann configuration as a function of angle of incidence. Reprinted with permission from H. J. Simon, D. E. Mitchell and J. G. Watson, *Phys. Rev. Lett.* **33** 1531 (1974). © 1974 by the American Physical Society. [46]

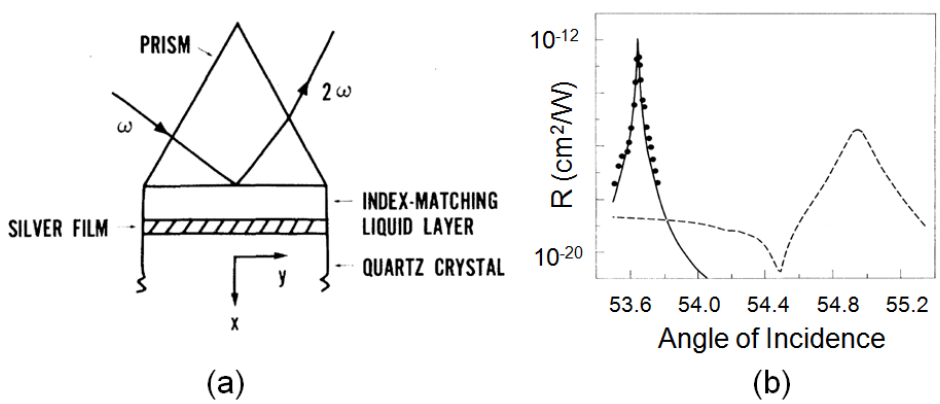

Fig. 12.22. Second harmonic generation at a silver surface in a hybrid prism configuration using long range SPs and a nonlinear quartz crystal. The experimental arrangement is shown in (a) and the results in (b). The dots are experimental measurements of the second harmonic reflection coefficient and are normalized to the solid curve which is the theoretical prediction. The dashed curve is the theoretical curve for a single-boundary SP. Reprinted with permission from J. C. Quail, J. G. Rako, H. J. Simon and R. T. Deck, *Phys. Rev. Lett.* **50** 1987-1989 (1983). © 1983 by the American Physical Society. [47]

12.7 Heat assisted magnetic recording

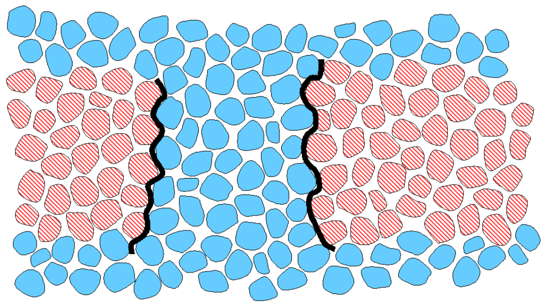

Fig. 12.23. Two magnetic transitions representing two bits of information in a granular magnetic recording medium. Due to the granularity of the medium, the transitions are not precisely sharp. Transition jitter can lead to errors in the recovered data. By making the grains smaller, the transitions become smoother and their location becomes more precise.

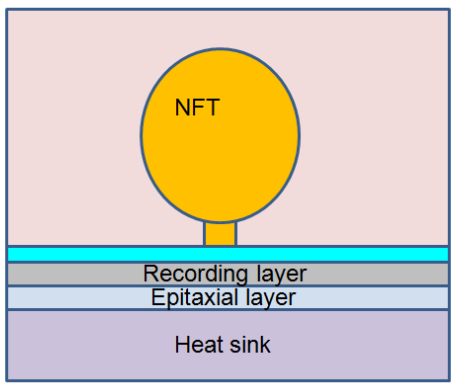

Fig. 12.24. Illustration of the "lollipop" SP NFT adjacent to the recording medium for HAMR. The disk of the NFT is about 200 nm in diameter, the peg is 50 nm wide and 15 nm long, and the NFT is about 25 nm thick. The recording medium consists of a thin film of a high coercivity FePt alloy grown epitaxially on a substrate that also acts as a heat sink. The gap between the bottom of the NFT and the the recording layer is ≤15 nm. [53]

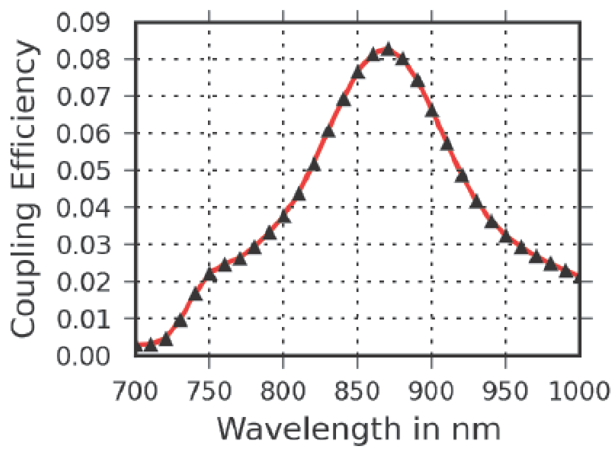

Fig. 12.25. Fraction of the optical power that is focused onto the NFT that is coupled into a 70 by 70 nm^2 region in the recording layer below the NFT as a function of wavelength. Courtesy A. Itagi and Seagate Technology. [53]

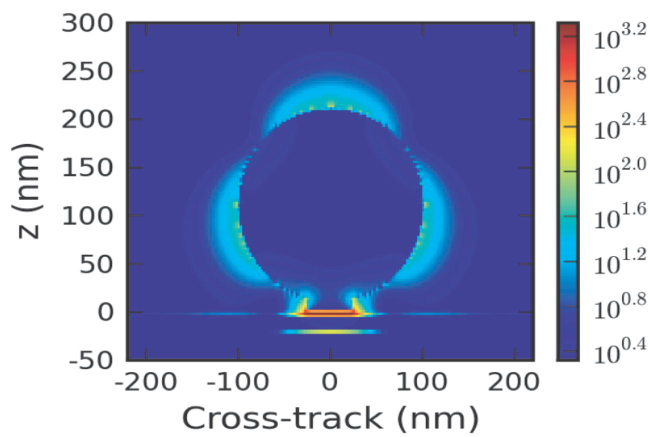

Fig. 12.26. $|E|^2$ field intensity around the lollipop transducer at resonance as computed by FDTD. Courtesy A. Itagi and Seagate Technology. [53]

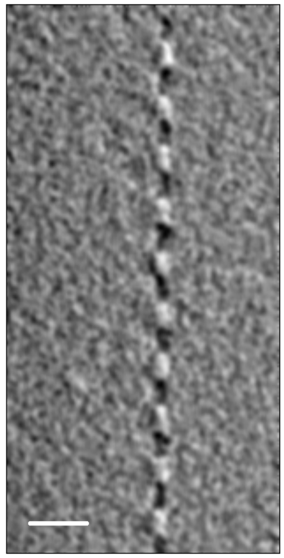

Fig. 12.27. Magnetic force microscope image of a track recorded on an FePt medium by HAMR. The full width at half maximum of the track was ~75 nm. The scale bar is 300 nm. Courtesy Seagate Technology. [53]

12.8 Nanophotonics

12.8.2 SP focusing

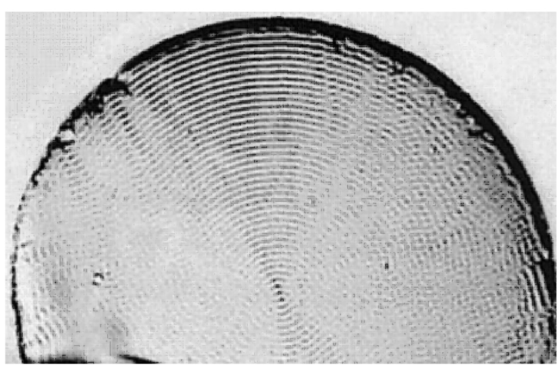

Fig. 12.28. SPs propagating on a gold film have been launched by edge coupling around the circumference. The incident beam is linearly polarized. The SP focusing is observable from the top edge down to the center of the sample by coating the gold with a thin layer of PMMA and illuminating the sample at a wavelength of 9.55 μm with sufficient power to heat the plastic and deform it. Used by permission of Blackwell Publishing Ltd. [60]

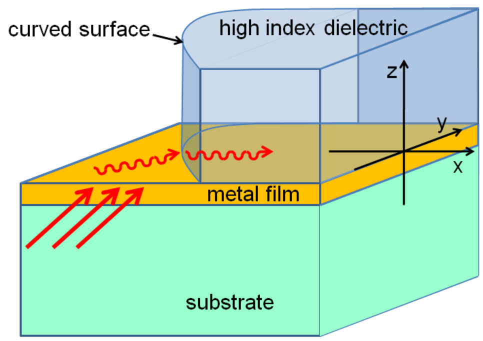

Fig. 12.29. Diagram of a structured thin film device for focusing SPs. The substrate is a transparent dielectric like glass. It is coated with a thin film of a plasmonic metal like gold. Light is incident from below along the red arrows through a prism in the Kretschmann configuration and excites a propagating SP indicated by the wavy line on the top surface of the metal film. When the propagating SP reaches the curved high index dielectric, its effective index increases. Therefore, the SP is refracted towards a focus.

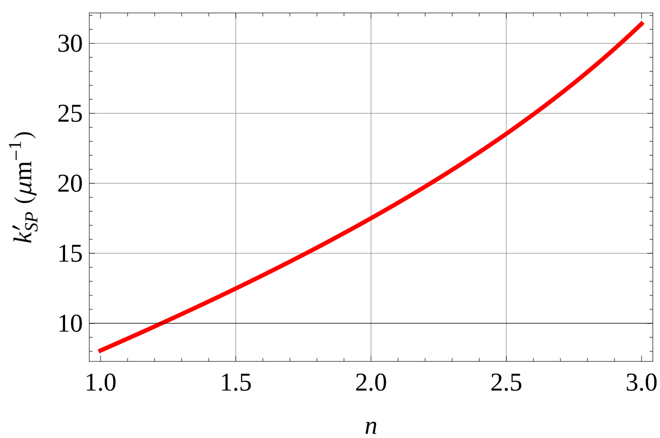

Fig. 12.30. SP wavevector on a gold surface at a wavelength of 800 nm as a function of the refractive index, n, of the dielectric on top of the gold. (*Mathematica* simulation.)

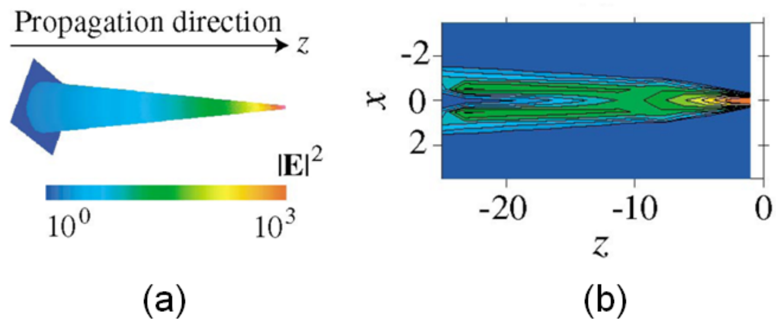

Fig. 12.31. SPs propagating down a sharp silver needle with a cone angle of 0.04 rad can generate electric field amplitudes that are three orders of magnitude greater than the incident field. *x* and *z* scales are in units of reduced wavelength so that the cone in reality tapers from 50 nm to 2 nm. The free space wavelength is 630 nm. (a) Geometry of the needle and (b) the electric field intensity $|E|^2$ in cross section. Reprinted with permission from M. Stockman, *Phys. Rev. Lett.* **93** 137404 (2004). © 2004 by the American Physical Society. [63]

12.8.3 SP channeling

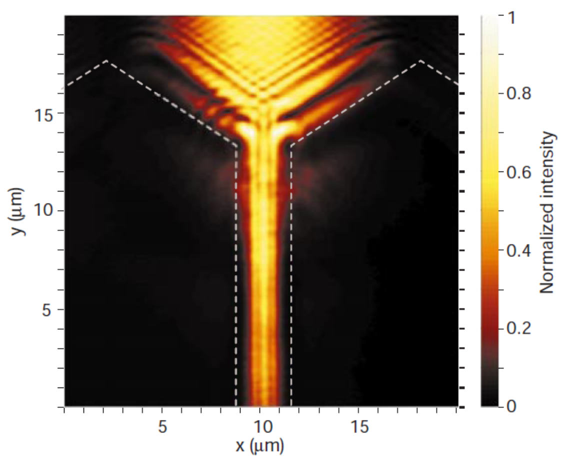

Fig. 12.32. SPs propagating down gold channel waveguide with a width of 2.5 μm. The incident laser wavelength is 800 nm. Reprinted by permission from Macmillan Publishers Ltd: *Nature* [59] © 2003.

12.8.4 Single holes and beaming

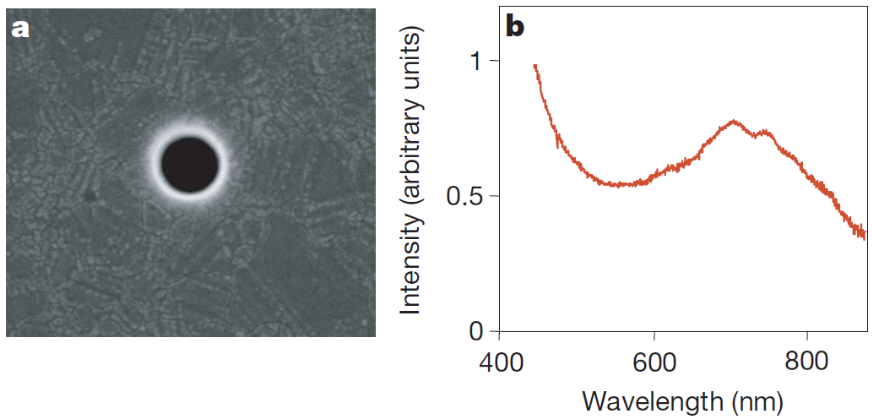

Fig. 12.33. (a) A 200 nm diameter hole in a 270 nm thick suspended silver film. Transmissivity spectrum for white light exhibitting a resonant enhancment at ~700 nm not predicted from Bethe's theory. Reprinted by permission from Macmillan Publishers Ltd: *Nature* [64], © 2007.

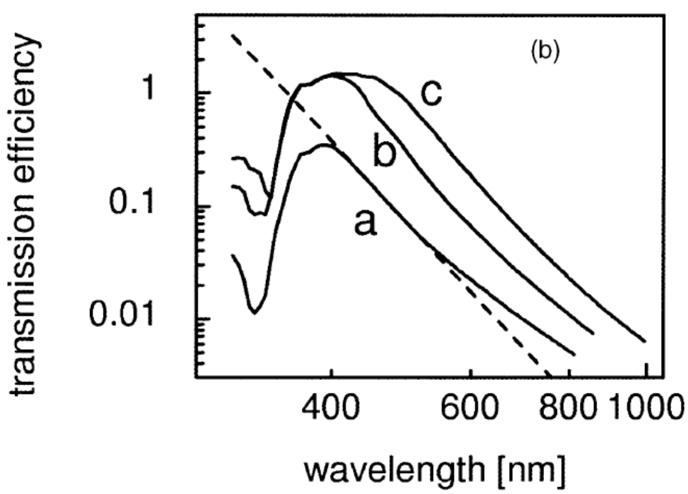

Fig. 12.34. Numerical calculation of transmission efficiency through a 100 nm hole in a 100 nm thick film of silver. Reprinted from *Opt. Commun.*, **195**, R. Wannemacher, "Plasmon-supported transmisson of light through nanometric holes in metallic thin films," 107. © 2001, with permission from Elsevier. [69]

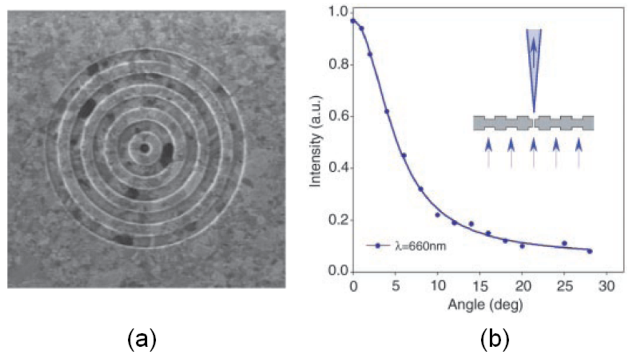

Fig. 12.35. (a) A single hole is surrounded by concentric grooves in a silver film. The hole diameter is 250 nm. The groove depth is 60 nm in a 300 nm thick film and the groove period is 500 nm. (b) Intensity of transmitted light as a function of angle at the peak transmission wavelength of 660 nm. From H. J. Lezec *et al.*, *Science* **297** (2002) 820. Reprinted with permission from AAAS. [70]

12.8.5 Hole arrays

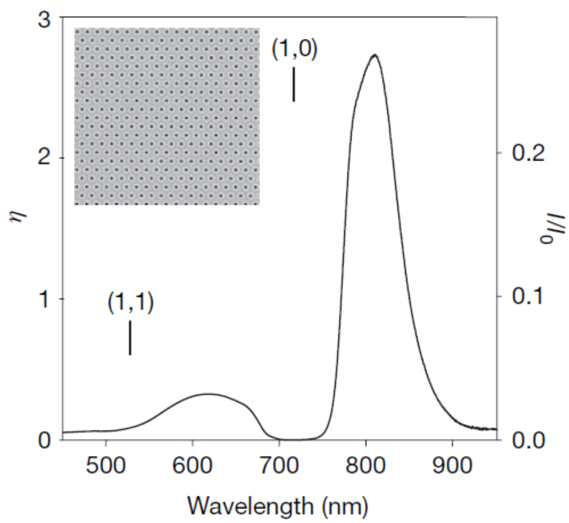

Fig. 12.36. Arrays of 170 nm holes in a triangular lattice with a 520 nm period in a 225 nm thick gold film. The substrate is glass and index matching fluid is placed on the other side of the film. The transmissivity spectrum at normal incidence indicates that at λ~800 nm nearly three times as much light is transmitted as is incident upon the open area of the holes. The scale on the right side of the graph is absolute transmission. Reprinted by permission from Macmillan Publishers Ltd: *Nature* [64], © 2007.

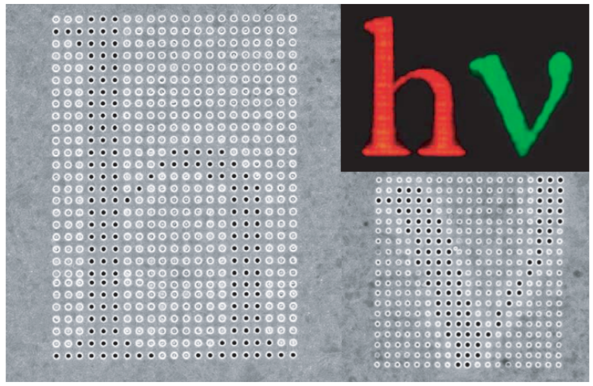

Fig. 12.37. Arrays of dimples in a silver film. On the left, the dimples have a period of 550 nm. On the right the period is 450 nm. Some of the dimples are milled through to make holes. When illuminated with white light, the period of the dimples makes the transmitted light red for "h" and green for "ν" as shown in the upper right inset (color in CD version). Reprinted by permission from Macmillan Publishers Ltd: *Nature* [64], © 2007.

12.8.6 SP interference

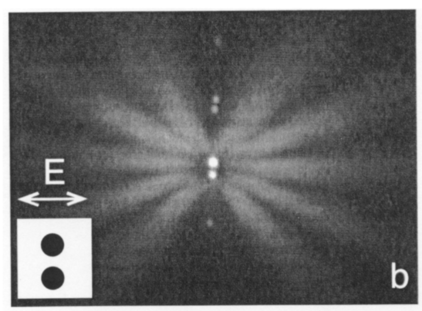

Fig. 12.38. Interference between SPs launched by light incident upon two 200 nm diameter silver nanoparticles, 60 nm high, at the center of the image. Light at a wavelength of 750 nm was focused onto the nanoparicles through a 50× microscope objective and polarized as shown in the figure. The particles lie on top of a silver surface which has been coated with a thin fluorescent layer to make the propagation of the SPs visible. Used by permission of Blackwell Publishing Ltd. [72]

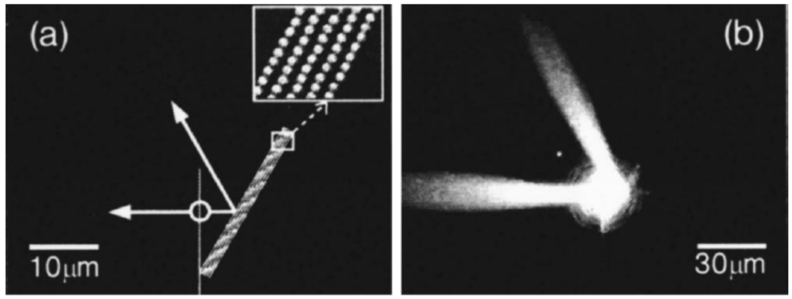

Fig. 12.39. (a) Light is focused onto a nanowire at the position of the circle. Light propagates both to the left and right. On the right, five rows of silver nanobumps form a Bragg reflector as shown in the inset. (b) The SPs propagating to left and right and SP reflection on the right by the mirror are clearly visible. Reprinted with permission from H. Ditlbacher, J. R. Krenn, G. Schider, A. Leitner and F. R. Aussenegg. *Appl. Phys. Lett.* **81** #10, 1762 (2002). © 2002, American Institute of Physics. [73]

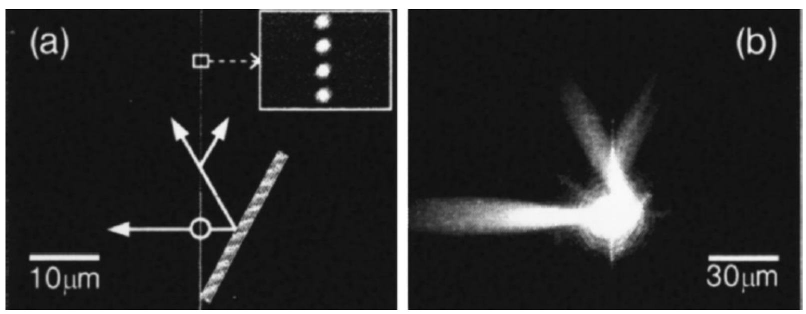

Fig. 12.40. (a) As in Fig. 12.39, light is focused onto a nanowire at the position of the circle. The light which propagates to the right is reflected by the Bragg reflector and is incident upon a single row of vertical silver nanobumps as shown in the inset where it is split into two beams. (b) The SP propagation is made visible by the fluorescent overcoat. Both the reflected and transmitted beam are visible at the beamsplitter. Reprinted with permission from H. Ditlbacher, J. R. Krenn, G. Schider, A. Leitner and F. R. Aussenegg. *Appl. Phys. Lett.* **81** #10, 1762 (2002). © 2002, American Institute of Physics. [73]

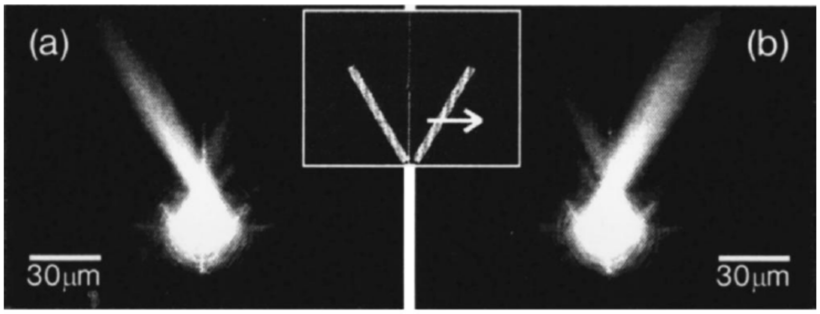

Fig. 12.41. Both SP beams are reflected to the beamsplitter. In (a) the path lengths are adjusted so that the SP beams constructively interfere at the beamsplitter for the beam propagating to the left while in (b) the beams constructively intefere to the right side of the beamsplitter. Reprinted with permission from H. Ditlbacher, J. R. Krenn, G. Schider, A. Leitner and F. R. Aussenegg. *Appl. Phys. Lett.* **81** #10, 1762 (2002). © 2002, American Institute of Physics. [73]

12.8.7 SP lasers

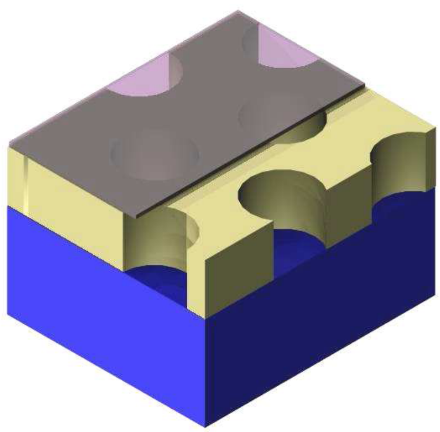

Fig. 12.42. Film structure that exhibited spectral line narrowing. The bottom blue layer is aluminum. The yellow layer is anodized aluminum oxide. Flourescein is placed within the holes, and the structure is overcoated with graphene. Used by permission. [74]

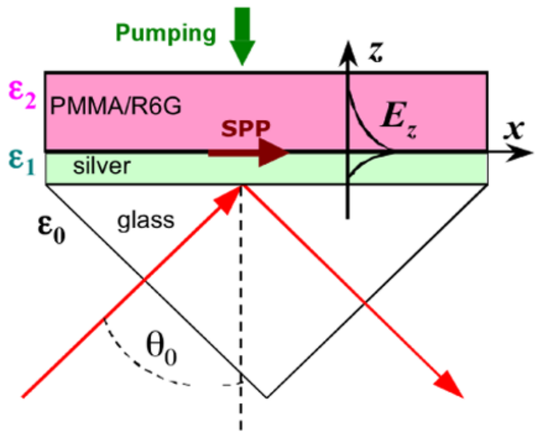

Fig. 12.43. Film structure that exhibited spectral line narrowing. The glass prism had an index of 1.7835. The silver film was 39 - 81 nm thick. This was coated with 1 to 3 μm of polymethyl methacrylate doped with rhodamine 6G at 2.2 × 10^{-2} M. Reprinted with permission from M. A. Noginov, G. Zhu, M. Mayy, B. A. Ritzo, N. Noginova and V. A. Podolskiy, *Phys. Rev. Lett.* **101** 226806 (2008). © 2008 by the American Physical Society. [75]

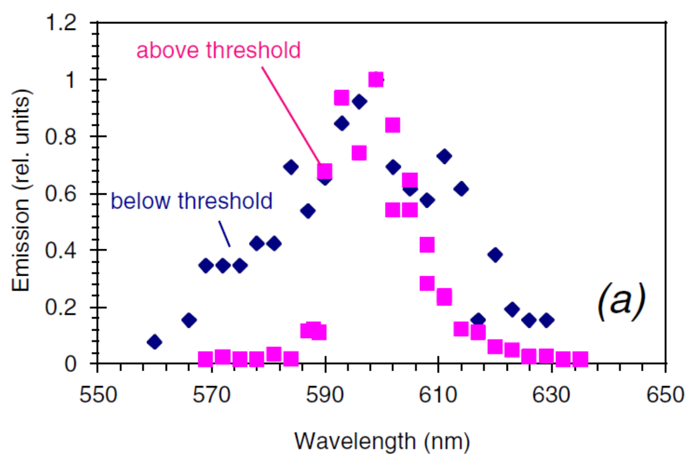

Fig. 12.44. Spectral narrowing in the light emission from SPs as seen from a low pump fluence (10.9 mJ/cm^2) and a high pump fluence (81.9 mJ/cm^2). Reprinted with permission from M. A. Noginov, G. Zhu, M. Mayy, B. A. Ritzo, N. Noginova and V. A. Podolskiy, *Phys. Rev. Lett.* **101** 226806 (2008). © 2008 by the American Physical Society. [75]

12.9 Cancer detection and treatment

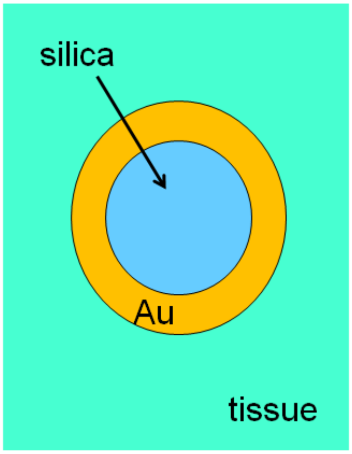

Fig. 12.45. Schematic of gold nanoshell embedded in tissue. In the study [78], the core diameter was 110 ± 11 nm and the shell thickness was 10 nm. The peak absorbance was at 820 nm.

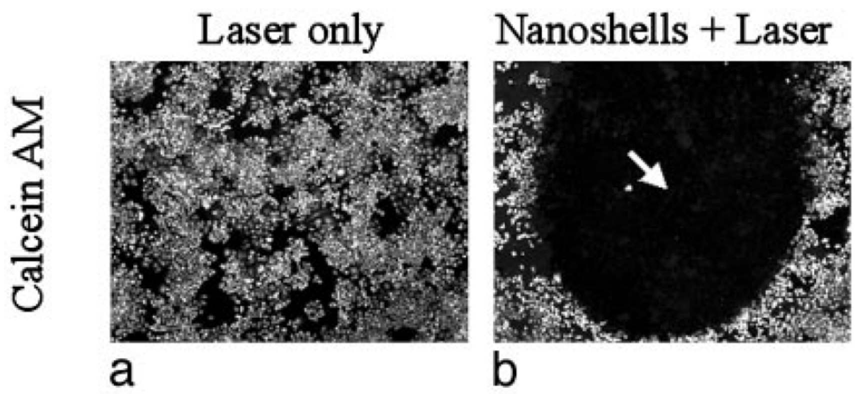

Fig. 12.46. (a) Cells without nanoshells irradiated with laser light. The image is from calcein fluorescence and is a sign that the cells are still viable. (b) Cells with nanoshells irradiated with laser light. A clear region is visible where the cells have died. Used by permission from L. R. Hirsch *et al.* *Proc. Nat. Acad. Sci.* **100** (2003) 13549. © 2003 National Academy of Sciences, U.S.A. [78]

12.10 Other applications

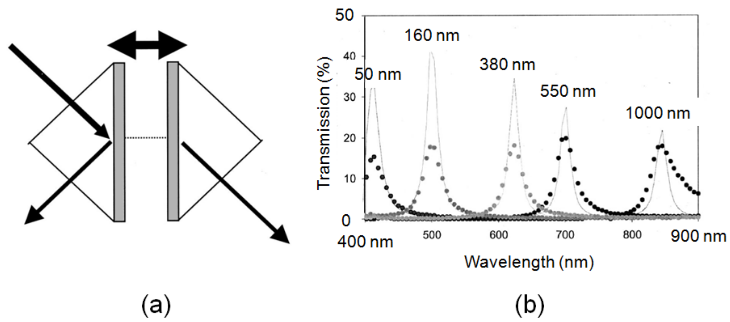

Fig. 12.47. (a) Optical design for a variable wavelength filter. (b) Measured transmissivity vs. gap distance between the prisms. Reprinted with permission from Y. Wang. *Appl. Phys. Lett.* **82** #24, 4385 (2003) © 2003, American Institute of Physics. [79]

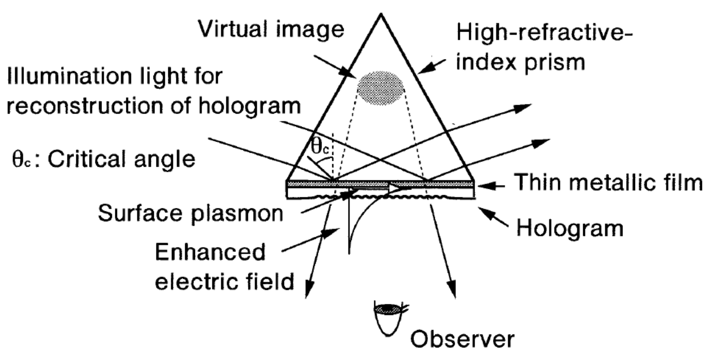

Fig. 12.48. Optical principle of the SP effect in holography. Used by permission. [80]

Fig. 12.49. "October, the Labours of the Months" stained glass window from Norwich, England, ca. 1480. © Victoria and Albert Museum, London. Used by permission.

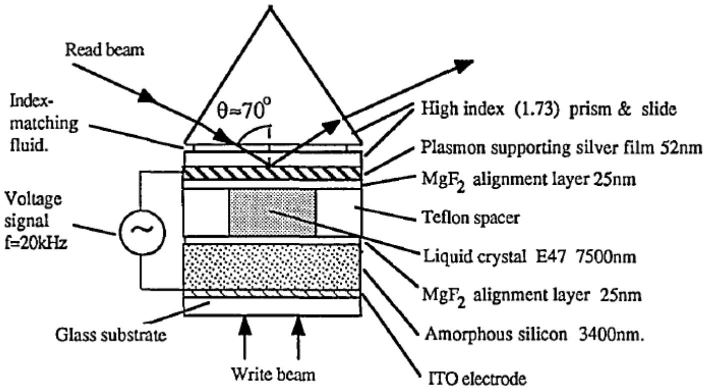

Fig. 12.50. Design for a liquid crystal and SP spatial light modulator. Used by permission. [81]

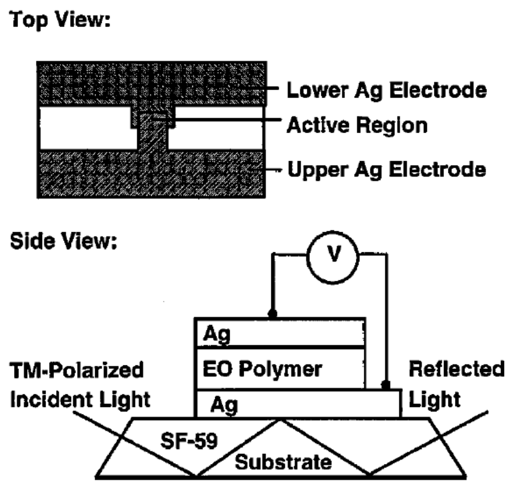

Fig. 12.51. Design for an electro-optic SP light modulator. Used by permission. [82]

Exercises

1. For a biosensor in the Kretschmann configuration with a gold sensing surface immersed in water (n = 1.33) at a wavelength of 830 nm, how much will the SP resonance angle shift when the local refractive index changes by 1×10^{-7}?

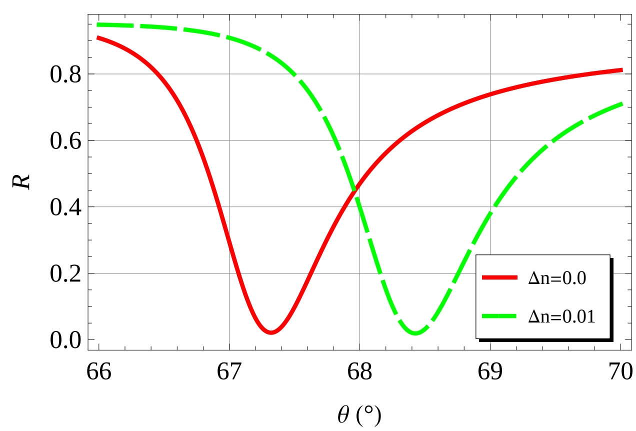

The minimum reflectivity angle of the resonance shifts from {67.32, 0.0209984} to {68.43, 0.018929} or 0.11° for Δn=0.01. An index change of 10^{-7} should therefore give a resonance angle shift of $\sim 10^{-6}$ degrees.

2. Using Mie theory, verify the statement in the text that the resonance wavelength shifts by about 200 nm per unit change in refractive index for silver nanoparticles in water (n = 1.33).

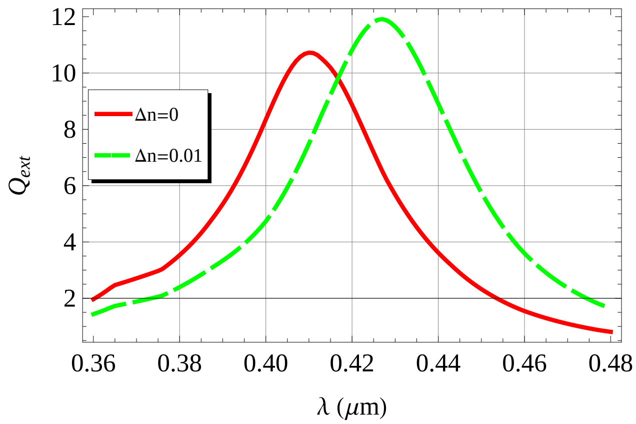

The resonance wavelength shifts from {0.41, 10.7236} to {0.427, 11.9139}, so $\Delta\lambda$=17 nm for Δn=0.1.

3. Compare the measured transmissivity spectrum in Fig. 12.12 for an optical fiber sensor with the theoretical reflectivity spectrum in the Kretschmann configuration. Assume that the silver film on the glass prism is 50 nm thick and that the angle of incidence is fixed at 75°. Compare both the linewidth of the resonance and the wavelength shift. Which type of SPR sensor is likely to be more sensitive and why?

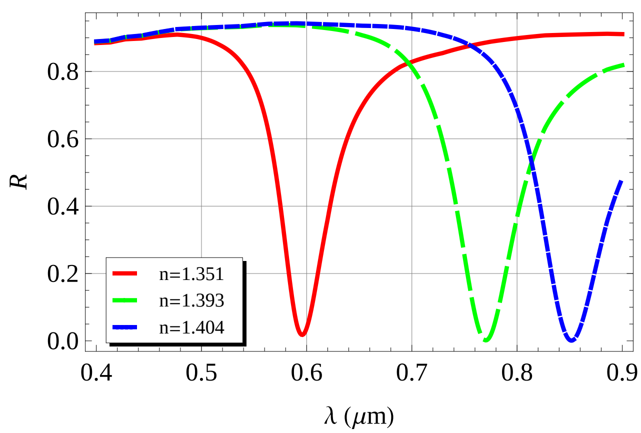

The Kretschmann configuration has both a narrower linewidth and a larger wavelength shift, so it will be more sensitive than the SPR optical fiber sensor. This is because the incident beam in the Kretschmann configuration is assumed to be at a single angle, while in the optical fiber the light incident upon the gold film from inside the core has a broader range of angles or wavevectors.

4. If the dielectric below a 50 nm metal film in the Kretschmann configuration is water with a refractive index of 1.33 instead of air, at what angle of incidence does the SP resonance occur for silver and gold at a wavelength of 800 nm? Is the field amplitude at the surface of the silver film larger with water in place of air, or smaller? Does the field penetrate further into an air dielectric or a water dielectric?

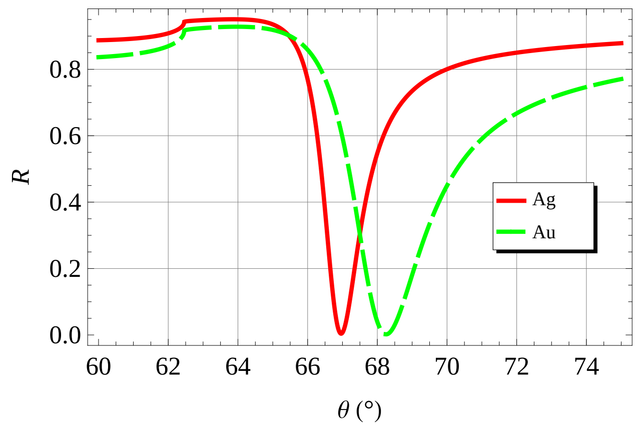

Exercise 4a. Reflectivity vs. polar angle for 50 nm silver and gold films in the Kretschmann configuration at λ = 800 nm.

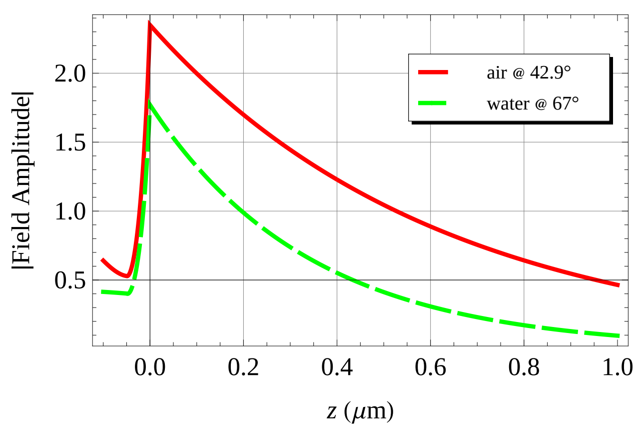

Exercise 4b: Field amplitudes vs. distance from the surface of a silver film in air and water.

References

[1] E. Kretschmann. Determination of the optical constants of metals by excitation of surface plasmons. *Z. Phys.* **241** (1971) 313.

[2] W. P. Chen and J. M. Chen. Use of surface plasma waves for determination of the thickness and optical constants of thin metallic films. *J. Opt. Soc. Am.* **71** (1981) 189.

[3] R. A. Innes and J. R. Sambles. Optical characterisation of gold using surface plasmon-polaritions. *J. Phys. F: Met. Phys.* **17** (1987) 277. Published by IOP Publishing Ltd.

[4] W. B. Lin, J. M. Chovelon, and N. Jaffrezic-Renault. Fiber-optic surface-plasmon resonance for the determination of thickness and optical constants of thin metal films. *Appl. Opt.* **39** (2000) 3261.

[5] C. Nylander, B. Liedberg, T. Lind. Gas detection by means of surface plasmon resonance. *Sensors & Actuators* **3** (1982/3) 79.

[6] T.M. Chinowsky, J.G. Quinn, D.U. Bartholomew, R. Kaiser, and J.L. Elkind. Performance of the Spreeta 2000 integrated surface plasmon resonance affinity sensor. *Sensors and Actuators B* **91** (2003) 266.

[7] Spreeta TSPR2KXY Biosensor Product Bulletin, Texas Instruments, http://www.sensata.com/sensors/spreeta-analytical-sensor-highlights.htm.

[8] Spreeta: the binding of neutravidin followed by the attachment of biotinylated antibodies to the Spreeta surface. Texas Instruments application brief 004 (1999) SLYA015A.

[9] A. D. McFarland and R. P. Van Duyne. Single silver nanoparticles as real-time optical sensors with zepto-mole sensitivity. *Nano Lett.* **3** (2003) 1057.

[10] D. S. Ginger, Y. C. Cao and C. A. Mirkin. Next-generation biosensing with gold nanoparticles. *Biophoton. Internat.* (July, **2003**) 48.

[11] R. C. Jorgenson, C. Jung, S. S. Yee and L. W. Burgess. Multi wavelength surface plasmon resonance as an optical sensor for characterizing the complex refractive indices of chemical samples. *Sens. Actuators B* **14** (1993) 721.

[12] W. A. Challener, R. R. Ollman and K. K. Kam. A surface plasmon resonance gas sensor in a 'compact disc' format. *Sens. Actuators B* **56** (1999) 254.

[13] R. C. Jorgenson and S. S. Yee. A fiber-optic chemical sensor based on surface-plasmon resonance. *Sens. Actuators B* **12** (1993) 213.

[14] J. Homola. Optical fiber sensor based on surface plasmon excitation. *Sens. Actuators B* **29** (1995) 401.

[15] M.Specht, J. D. Pedarnig, W. M. Heckl and T. W. Hänsch. Scanning plasmon near-field microscope. *Phys. Rev. Lett.* **68** (1992) 476.

[16] S. I. Bozhevolnyi, B. Vohnsen, I. I. Smolyaninov, A. V. Zayats. Direct observation of surface polariton localization caused by surface roughness. *Opt. Commun.* **117** (1995) 417.

[17] O. Sqalli, I. Utke, P. Hoffmann and F. Marquis-Weible. Gold elliptical nanoantennas as probes for near field optical microscopy. *J. Appl. Phys.* **92** (2002) 1078.

[18] T. Thio, H.J. Lezec, T. W. Ebbesen. Strongly enhanced optical transmission through subwavelength holes in metal films. *Physica B* **279** (2000) 90.

[19] J. B. Pendry. Negative refraction makes a perfect lens. *Phys. Rev. Lett.* **85** (2000) 3966.

[20] N. Fang, Z. W. Liu, T. J. Yen and X. Zhang. Regenerating evanescent waves from a silver superlens. *Opt. Exp.* **11** (2003) 682.

[21] N. Fang, H. Lee, C. Sun and X. Zhang. Sub-diffraction-limited optical imaging with a silver superlens. *Science* **308** (2005) 534.

[22] H. Lee, Y. Xiong, N. Fang, W. Srituravanich, S. Durant, M. Ambati, C. Sun and X. Zhang. Realization of optical superlens imaging below the diffraction limit. *New J. Phys.* **7** (2005) 255.

[23] Z. Jacob, L. V. Alekseyev and E. Narimanov. *Optical Hyperlens*: Far-field imaging beyond the diffraction limit. *Opt. Exp.* **14** (2006) 8247.

[24] Z. Liu, H. Lee, Y. Xiong, C. Sun and X. Zhang. Far-field optical hyperlens magni-

fying sub-diffraction-limited objects. *Science* **315** (2007) 1686.

[25] H. Lee, Z. Liu, Y. Xiong, C. Sun and X. Zhang. Development of optical hyperlens for imaging below the diffraction limit. *Opt. Exp.* **15** (2007) 15886.

[26] I. I. Smolaninov, Y. J. Hung and C. C. Davis. Magnifying superlens in the visible frequency range. *Science* **315** (2007) 1699.

[27] G. Shvets, S. Trendafilov, J. B. Pendry and A. Sarychev. Guiding, focusing, and sensing on the subwavelength scale using metallic wire arrays. *Phys. Rev. Lett.* **99** (2007) 53903.

[28] S. Kawata, A. Ono and P. Verma. Subwavelength colour imaging with a metallic nanolens. *Nat. Photon.* **2** (2008) 438.

[29] S. Kawata, Y. Inouye and P. Verma. Plasmonics for near-field nano-imaging and superlensing. *Nat. Photon.* **3** (2009) 388.

[30] M. Fleischmann, P. J. Hendra and A. J. McQuillan. Raman spectra of pyridine adsorbed at a silver electrode. *Chem. Phys. Lett.* **26** (1974) 163.

[31] M. Moskovits. Surface-enhanced spectroscopy. *Rev. Mod. Phys.* **57** (1985) 783.

[32] D. I. Jeanmaire and R. P. Van Duyne. Surface Raman electrochemistry. Part I. Heterocyclic, aromatic and aliphatic amines adsorbed on the anodized silver electrode. *J. Electroanal. Chem.* **84** (1977) 1.

[33] M. G. Albrecht and J. A. Creighton. Anomalously intense Raman spectra of pyridine at a silver electrode. *J. Am. Chem. Soc.* **99** (1977) 5215.

[34] H. Xu, J. Aizpurua, M. Kall and P. Apell. Electromagnetic contributions to single-molecule sensitivity in surface-enhanced Raman scattering. *Phys. Rev. E* **62** (2000) 4318.

[35] A. Otto, I. Mrozek, H. Grabhorn and W. Akemann. Surface-enhanced Raman scattering. *J. Phys.: Condens. Matter* **4** (1992) 1143.

[36] J. Gersten and A. Nitzan. Electromagnetic theory of enhanced Raman scattering by molecules adsorbed on rough surfaces. *J. Chem Phys.* **73** (1980) 3023.

[37] G. Boas. Collidal particles improve surface-enhanced Raman scattering. *Biophoton. Intl.* (January, 2004) 65.

[38] R. G. Freeman, K. C. Grabar, K. J. Allison, R. M. Bright, J. A. Davis, A. P. Guthrie, M. B. Hommer, M. A. Jackson, P. C. Smith, D. G. Walter and M. J. Natan. Self-assembled metal colloid monolayers: an approach to SERS substrates. *Science* **267** (1995) 1629.

[39] F. J. García-Vidal and J. B. Pendry. Collective theory for surface enhanced Raman scattering. *Phys. Rev. Lett.* **77** (1996) 1163.

[40] M. Kerker, D.-S. Wang and H. Chew. Surface enhanced Raman scattering (SERS) by molecules adsorbed at spherical particles. *Appl. Opt.* **19** (1980) 3373.

[41] C. L. Haynes and R. P. Van Duyne. Plasmon-sampled surface-enhanced Raman excitation spectroscopy. *J. Phys. Chem.* B **107** (2003) 7426.

[42] K. Kneipp, Y. Wang, H. Kneipp, L. T. Perelman, Irving Itzkan, R. R. Dasari, and M. S. Feld. Single molecule detection using surface-enhanced Raman scattering (SERS). *Phys. Rev. Lett.* **78** (1997) 1667.

[43] S. Nie and S. R. Emory. Probing single molecules and single nanoparticles by surface-enhanced Raman scattering. *Science* **275** (1997) 1102.

[44] J. Grand, M. L. de la Chapelle, J.-L. Bijeon, P.-M. Adam, A. Vial and P. Royer. Role of localized surface plasmons in surface-enhanced Raman scattering of shape-controlled metallic particles in regular arrays. *Phys. Rev. B* **72** (2005) 033407.

[45] M. Kerker. Founding fathers of light scattering and surface-enhanced Raman scattering. *Appl. Opt.* **30** (1991) 4699.

[46] H. J. Simon, D. E. Mitchell and J. G. Watson. Optical second-harmonic generation with surface plasmons in silver films. *Phys. Rev. Lett.* **33** (1974) 1531.

[47] J. C. Quail, J. G. Rako, H. J. Simon and R. T. Deck. Optical second-harmonic generation with long-range surface-plasmons. *Phys. Rev. Lett.* **50** (1983) 1987.

[48] A. Bouhelier, M. Beversluis, A. Hartschuh, and L. Novotny. Near-field second-harmonic generation induced by local field enhancement. *Phys. Rev. Lett.* **90** (2003)

013903.

[49] D. Sarid, R. T. Deck and J. J. Fasano. Enhanced nonlinearity of the propagation constant of a long-range surface-plasma wave. *J. Opt. Soc. Am.* **72** (1982) 1345.

[50] Y. J. Chen and G. M. Carter. Measurement of third order nonlinear susceptibilities by surface plasmons. *Appl. Phys. Lett.* **41** (1982) 307.

[51] M. H. Kryder, E. C. Gage, T. W. McDaniel, W. A. Challener, R. E. Rottmayer, G. Ju, Y-T. Hsia and M. F. Erden. Heat assisted magnetic recording. *Proc. IEEE* **96 (**2008) 1810.

[52] L. Néel. Théorie du traînage magnétique des ferromagnétiques en grains fins avec applications aux terres cuites. *Ann. Géophys.* **5** (1949) 99.

[53] W. A. Challener, C. Peng, A. V. Itagi, D. Karns, W. Peng, Y. Peng, X. Yang, X. Zhu, N. J. Gokemeijer, Y.-T. Hsia, G. Ju, R. E. Rottmayer, M. A. Seigler and E. C. Gage. Heat-assisted magnetic recording by a near-field transducer with efficient optical energy transfer. *Nature Phot.* **3** (2009) 220.

[54] W. A. Challener, C. Mihalcea, C. Peng, and K. Pelhos. Miniature planar solid immersion mirror with focused spot less than a quarter wavelength. *Opt. Exp.* **13**, (2005) 7189.

[55] L. Novotny and B. Hecht. *Principles of Nano-Optics* (Cambridge: Cambridge University Press, 2006).

[56] P. N. Prasad. *Principle of Nanophotonics* (Hoboken: John Wiley & Sons, 2004).

[57] V. M. Shalaev and S. Kawata, eds. *Nanophotonics with Surface Plasmons* (Amsterdam: Elsevier, 2007).

[58] M. L. Brongersma and P. G. Kik, eds. *Surface Plasmon Nanophotonics* (Dordrecht: Springer, 2007).

[59] W. L. Barnes, A. Dereux and T. W. Ebbesen. Surface plasmon subwavelength optics. *Nature* **424** (2003) 824.

[60] F. Keilmann. Surface-polariton propagation for scanning near-field optical microscopy application. *J. Microsc.* **194** (1999) 567.

[61] J. M. Steele, Z. Liu, Y. Wang and X. Zhang. Resonant and non-resonant generation and focusing of surface plasmons with circular gratings. *Opt. Exp.* **14** (2006) 5664.

[62] W. A. Challener. Surface plasmon lens for heat assisted magnetic recording. US2003/0128634 patent application (July 10, 2003).

[63] M. Stockman. Nanofocusing of optical energy in tapered plasmonic waveguides. *Phys. Rev. Lett.* **93** (2004) 137404.

[64] C. Genet and T. W. Ebbesen. Light in tiny holes. *Nature* **445** (2007) 39.

[65] H. A. Bethe. Theory of diffraction by small holes. *Phys. Rev.* **66** (1944) 163.

[66] T. W. Ebbesen, H. J. Lezec, H. F. Ghaemi, T. Thio, and P. A. Wolff. Extraordinary optical transmission through sub-wavelength hole arrays. *Nature* **391** (1998) 667.

[67] H. F. Ghaemi, Tineke Thio, D. E. Grupp, T. W. Ebbesen and H. J. Lezec. Surface plasmons enhance optical transmission through subwavelength holes. *Phys. Rev. B* **58** (1998) 6779.

[68] A. Degiron, H. J. Lezec, N. Yamamoto and T. W. Ebbesen. Optical transmission properties of a single subwavelength aperture in a real metal. *Opt. Commun.* **239** (2004) 61.

[69] R. Wannemacher. Plasmon-supported transmission of light through nanometric holes in metallic thin films. *Opt. Commun.* **195** (2001) 107.

[70] H. J. Lezec, A. Degiron, E. Devaux, R. A. Linke, L. Martin-Moreno, F. J. Garcia-Vidal, and T. W. Ebbesen. Beaming light from a subwavelength aperture. *Science* **297** (2002) 820.

[71] M. Sarrazin, J.-P. Vigneron and J.-M. Vigoureux. Role of Wood anomalies in optical properties of thin metallic films with a bidimensional array of subwavelength holes. *Phys. Rev. B* **67** (2003) 085415.

[72] J. R. Krenn, H. Ditlbacher, G. Schider, A. Hohenau, A. Leitner and F. R. Aussenegg. Surface plasmon micro- and nano-optics. *J. Microsc.* **209** (2003) 167.

[73] H. Ditlbacher, J. R. Krenn, G. Schider, A. Leitner and F. R. Aussenegg. Two-

dimensional optics with surface plasmon polaritons. *Appl. Phys. Lett.* **81** (2002) 1762.

[74] R. Li, A. Banerjee and H. Grebel. The possibility for surface plasmon lasers. *Opt. Exp.* **17** (2009) 1622.

[75] M. A. Noginov, G. Zhu, M. Mayy, B. A. Ritzo, N. Noginova and V. A. Podolskiy. Stimulated emission of surface plasmon polaritons. *Phys. Rev. Lett.* **101** (2008) 226806.

[76] A. Kumar, S. F. Yu, X. F. Li and S. P. Lau. Surface plasmonic lasing via the amplification of coupled surface plasmon waves inside dielectric-metal-dielectric waveguides. *Opt. Exp.* **16** (2008) 16113.

[77] D. J. Bergman and M. I. Stockman. Surface plasmon amplification by stimulated emission of radiation: quantum generation of coherent surface plasmons in nanosystems. *Phys. Rev. Lett.* **90** (2003) 027402.

[78] L. R. Hirsch, R. J. Stafford, J. A. Bankson, S. R. Sershen, B. Rivera, R. E. Price, J. D. Hazle, N. J. Halas and J. L. West. Nanoshell-mediated near-infrared thermal therapy of tumors under magnetic resonance guidance. *Proc. Nat. Acad. Sci.* **100** (2003) 13549.

[79] Y. Wang. Wavelength selection with coupled surface plasmon waves. *Appl. Phys. Lett.* **82** (2003) 4385.

[80] S. Maruo, O. Nakamura and S. Kawata. Evanescent-wave holography by use of surface-plasmon resonance. *Appl. Opt.* **36** (1997) 2343.

[81] M. E. Caldwell and E. M. Yeatman. Surface-plasmon spatial light modulators based on liquid crystal. *Appl. Opt.* **31** (1992) 3880.

[82] C. Jung, S. Yee, and K. Kuhn. Electro-optic polymer light modulator based on surface plasmon resonance. *Appl. Opt.* **34** (1995) 946.